Dynactin p150 promotes processive motility of DDB complexes by minimizing diffusional behavior of dynein

Qingzhou Feng[a,b], Allison M. Gicking[a], and William O. Hancock[a,b,*]
[a]Department of Biomedical Engineering and [b]Molecular Cellular and Integrative Biological Sciences Program, Huck Institute of Life Sciences, Pennsylvania State University, University Park, PA 16802

ABSTRACT **Cytoplasmic dynein is activated by forming a complex with dynactin and the adaptor protein BicD2. We used interferometric scattering (iSCAT) microscopy to track dynein–dynactin–BicD2 (DDB) complexes in vitro and developed a regression-based algorithm to classify switching between processive, diffusive, and stuck motility states. We find that DDB spends 65% of its time undergoing processive stepping, 4% undergoing 1D diffusion, and the remaining time transiently stuck to the microtubule. Although the p150 subunit was previously shown to enable dynactin diffusion along microtubules, blocking p150 enhanced the proportion of time DDB diffused and reduced the time DDB processively walked. Thus, DDB diffusive behavior most likely results from dynein switching into an inactive (diffusive) state, rather than p150 tethering the complex to the microtubule. DDB–kinesin-1 complexes, formed using a DNA adapter, moved slowly and persistently, and blocking p150 led to a 70 nm/s plus-end shift in the average velocity of the complexes, in quantitative agreement with the shift of isolated DDB into the diffusive state. The data suggest a DDB activation model in which dynactin p150 enhances dynein processivity not solely by acting as a diffusive tether that maintains microtubule association, but rather by acting as an allosteric activator that promotes a conformation of dynein optimal for processive stepping. In bidirectional cargo transport driven by the opposing activities of kinesin and dynein–dynactin–BicD2, the dynactin p150 subunit promotes retrograde transport and could serve as a target for regulators of transport.**

Monitoring Editor
Erika Holzbaur
University of Pennsylvania

Received: Sep 6, 2019
Revised: Jan 8, 2020
Accepted: Jan 28, 2020

INTRODUCTION

Intracellular transport is carried out by kinesin and cytoplasmic dynein motors that walk in opposite directions along microtubules, allowing for efficient bidirectional movement of cargo (Gross *et al.*, 2002; Nobutaka *et al.*, 2010; Hancock, 2014). Most cellular cargoes have both kinesin motors and dynein motors bound to them (Ligon *et al.*, 2004; Hendricks *et al.*, 2010), suggesting that robust coordination between, and regulation of, the opposite-polarity motors is required for transport; however, the underlying mechanisms are not clear. The currently prevailing model is the tug-of-war (Müller *et al.*, 2008; Hendricks *et al.*, 2010), in which ensembles of oppositely directed kinesins and dyneins compete, and the stronger motor team determines the directionality. The manner in which motor activity is regulated, via binding partners or posttranslational modifications, in the context of tug-of-war is not well understood. The tug-of-war model also does not properly account for the growing evidence that motor activity can be regulated via binding partners, and posttranslational modifications of the microtubule tracks (Belyy *et al.*, 2017; Monroy *et al.*, 2018). A more complete picture of intracellular transport must include the mechanisms by which kinesin and dynein coordinate their antagonistic activities. However, understanding this coordination first requires a more precise characterization of the individual motors, and how their activities are regulated.

This article was published online ahead of print in MBoC in Press (http://www.molbiolcell.org/cgi/doi/10.1091/mbc.E19-09-0495) on February 5, 2020.
The authors declare no conflict of interest.
Author contributions: Q.F. and W.O.H. designed research. Q.F. performed experiments and wrote the algorithm. A.M.G. and Q.F. carried out iSCAT experiments and image processing. Q.F. wrote the paper and Q.F., W.O.H., and A.M.G. edited the paper.
*Address correspondence to: William O. Hancock (wohbio@engr.psu.edu).
Abbreviations used: ATP, adenosine triphosphate; CTT, C-terminal tail of tubulin; DDB, dynein–dynactin–BicD2; GBP, GFP binding protein; GFP, green fluorescent protein; iSCAT, interferometric scattering; TIRF, total internal reflection fluorescence.

Due to its diverse cellular functions, cytoplasmic dynein is known to be regulated through binding to a wide array of cargo adapter proteins (Olenick and Holzbaur, 2019), a confounding factor in the effort to understand its motility. In contrast to its counterpart in yeast, it was recently discovered that mammalian dynein requires activating adapter proteins to achieve robust motility and substantial force generation in vitro (King and Schroer, 2000; Trokter *et al.*, 2012). Isolated dynein adopts an inhibited phi state in which one motor domain is rotated 180° with respect to the other and the two microtubule binding domain stalks are crossed, preventing microtubule binding and motility (Zhang *et al.*, 2017). Structural studies show that, when bound to its cofactor dynactin and the cargo adaptor BicD2, the dynein motor domains are released from the phi state and exist in an "open" conformation where they are either in a "parallel" arrangement optimal for processive walking, or in an "inverted" arrangement that allows microtubule binding but poor motility (Zhang *et al.*, 2017). BicD2 is a coiled-coil homodimer that lies along the dynactin filament and tightly links the dynein tail to dynactin, which constrains the orientation of the dynein heads and likely stabilizes the parallel conformation (Splinter *et al.*, 2012; Urnavicius *et al.*, 2015, 2018; Sladewski *et al.*, 2018). Evidence for this stabilization comes from single-molecule assays, where DDB complexes shows robust landing activity, superprocessivity, and considerably higher stall forces than dynein–dynactin or dynein alone (McKenney *et al.*, 2014; Belyy *et al.*, 2017). However, a molecular description of how BicD2 and related adapters such as BicDR, Hook3, and Spindly work together with dynactin to activate dynein is still being resolved (McKenney *et al.*, 2014; Schroeder and Vale, 2016; Belyy *et al.*, 2017).

A notable characteristic of activated dynein complexes in vitro is the broad distribution of measured velocities (Olenick *et al.*, 2016; Gutierrez *et al.*, 2017). As less than half of DDB complexes were observed to be in the activated open-parallel conformation by CryoEM (Zhang *et al.*, 2017), one explanation for this heterogeneity is that the motors switch between active and inactive states on a timescale faster than the experimental time resolution. This switching could produce periods of processive stepping interspersed with periods of pausing or 1D diffusion with zero net speed; thus, the overall speed would reflect the fraction of time the motor spends in an activated state. But what could cause this switch? One candidate is the dynactin p150 subunit, which contains a flexible linker terminating in a positively charged CAP-Gly domain that can interact with the microtubule and is known to affect dynein motility (King and Schroer, 2000; Ayloo *et al.*, 2014). However, the mechanism underlying this dynein velocity heterogeneity has not been investigated in detail due to a lack of high-resolution motility data and appropriate analysis tools to objectively separate the different motility states.

Here, we apply high-resolution particle tracking and a novel switch-point detection algorithm to investigate the mechanism of dynein activation by BicD2 and dynactin. Consistent with previous observations (McKenney *et al.*, 2014; Belyy *et al.*, 2017; Grotjahn *et al.*, 2018; Urnavicius *et al.*, 2018), DDB transitions between processive, diffusive, and stuck states. The stuck and diffusive episodes could be entirely due to p150-microtubule interactions; alternatively, they could reflect dynein being in an inhibited state that retains microtubule binding. We explored these two possibilities using a p150 antibody, previously shown to inhibit p150 interaction with microtubules (King and Schroer, 2000; Ross *et al.*, 2006). We found that blocking p150 led to longer and more frequent diffusive episodes and shorter processive episodes, suggesting that the diffusive behavior of DDB results from the dynein heads rather than from p150. When DDB was complexed with kinesin-1 using a DNA adapter, blocking p150 led to a plus-ended shift in the mean velocities, in quantitative agreement with the switching behavior of DDB alone. Thus, we conclude that dynactin subunit p150 acts as an allosteric activator of dynein that accelerates switching from, and helps prevent a return to, its inhibited state.

RESULTS

Purified DDB complexes display diverse motility behavior

DDB complexes were purified from bovine brain lysate by adding recombinant mouse BicD2 (25–400 aa; McKenney *et al.*, 2014) that lacks the inhibitory C-terminal domain, binding the complexes to Strep-Tactin beads (IBA Lifesciences), and eluting from the beads with *d*-Desthiobiotin (Sigma-Aldrich; Figure 1, A and B;

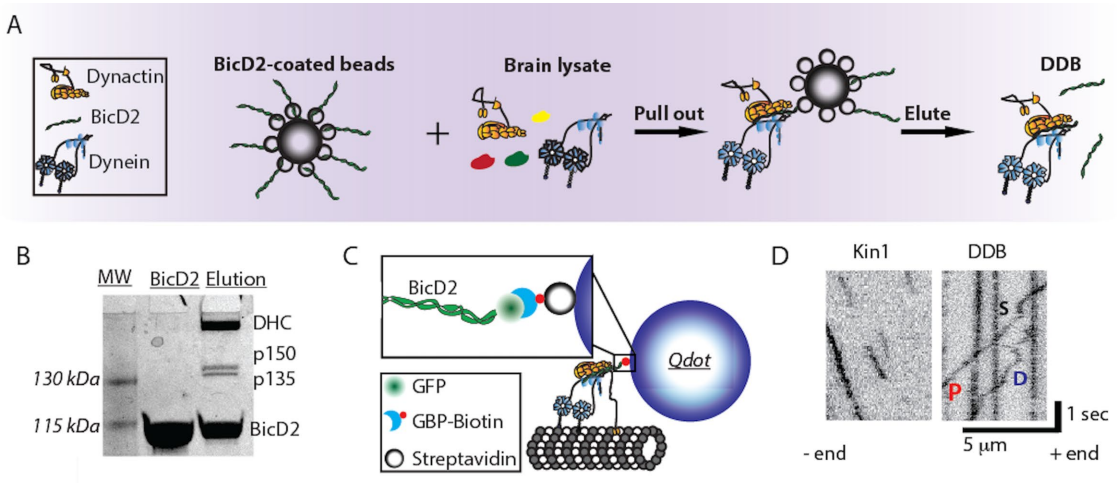

FIGURE 1: Purified DDB complex demonstrates processive, diffusive, and stuck behaviors. (A) Schematic of DDB purification using BicD2-coated Strep-Tactin beads to pull dynein/dynactin from brain lysate. DDB was then eluted off of the bead. (B) SDS–PAGE gel of recombinant BicD2 and final purified DDB complex showing dominant bands of dynein heavy chain (DHC), dynactin components p150 and p135, and BicD2. (C) Tagging DDB for single-molecule tracking. Biotinylated GFP binding protein (GBP) is used to link C-terminal GFP on BicD2 to streptavidin-coated quantum dots for TIRF experiments or streptavidin-coated 30-nm gold nanoparticles for iSCAT experiments. (D) Kymograph of kinesin-1 (left) and DDB (right) single-molecule motility. DDB displays processive runs (P), diffusive episodes (D), and stuck events (S).

McKenney *et al.*, 2014). The purified DDB contained a C-terminal GFP on BicD2 for visualization, but for enhanced spatiotemporal resolution, we attached streptavidin-functionalized quantum dots (Qdots) through a biotinylated GFP binding protein (GBP) nanobody (Figure 1C; see *Materials and Methods* for details; Kubala *et al.*, 2010). Using total internal reflection fluorescence (TIRF) microscopy with 50 ms exposure time, we tracked the motility of single DDB complexes along surface-immobilized microtubules and compared them to kinesin-1. Whereas kinesin-1 displayed runs with uninterrupted motility, DDB displayed three different motility behaviors: processive runs, diffusional episodes, and stuck segments where no movements were detected (Figure 1D). These behaviors have been observed in published DDB traces, but studies to date have generally focused only on segments of processive motility (McKenney *et al.*, 2014; Belyy *et al.*, 2017).

Blocking dynactin p150 alters DDB landing and motility

The p150 subunit of dynactin, which on its own can diffuse along microtubules, has been proposed to act as a tether that promotes microtubule binding and diffusional behavior of dynein–dynactin complexes, but its role in the DDB complex is not clear (Ayloo *et al.*, 2014; McKenney *et al.*, 2014, 2016; Schlager *et al.*, 2014; Tripathy *et al.*, 2014). To characterize how dynactin p150 alters DDB function, we utilized a p150 antibody (Ab_{p150}) that has previously been shown to block the interaction of p150 with microtubules (King and Schroer, 2000; Payne *et al.*, 2003; Ross *et al.*, 2006; Dixit *et al.*, 2008; Ayloo *et al.*, 2014), and compared the DDB motility in the absence and presence of Ab_{p150}. We first asked what role p150 plays in the initial landing of DDB to the microtubule. Based on its tethering activity, it could enhance landing by making first contact with the microtubule and allowing the dynein heads to bind; alternatively, the runs could be all initiated by dynein heads binding (Figure 2A). In the presence of p150 antibody, the DDB landing frequency decreased by roughly threefold compared with no antibody control (Figure 2, B and C) or a control antibody (Supplemental Figure S1A). This result, consistent with previous observations (Lloyd *et al.*, 2012; Moughamian and Holzbaur, 2012; Ayloo *et al.*, 2014; McKenney *et al.*, 2016), suggests that the initial encounter of DDB with the microtubule usually occurs through p150, although more complex mechanisms are possible. Because our DDB preparation contained a subfraction of p135 (Figure 1B), an isoform that lacks the CAP-Gly domain, it is possible that a fraction of the remaining landing events in the presence of p150 antibody represent complexes containing p135 rather than p150, meaning that our measurements provide a lower bound of the antibody effect.

We next asked how, following the initial landing of DDB on the microtubule, p150 influences dynein motility. To analyze dynein motility, the observed landing events were separated into three classes: stuck (S) complexes moved less than 100 nm overall; diffusive (D) complexes moved bidirectionally more than 100 nm for both directions with no observed unidirectional processive segments longer than 350 nm; and processive (P) complexes contained at least one segment of unidirectional movement longer than 350 nm (Figure 2D). For control DDB, roughly half of the complexes that landed displayed processive motility, and the rest were split between diffusive and stuck (Figure 2E). Blocking dynactin p150 with the antibody reduced the frequency of processive molecules by half, and reduced the number of diffusional and stuck complexes to near zero (Figure 2E). A simple interpretation of the drop in processive events is that half of these events occur when dynein initially contacts the microtubule and the other half when dynactin p150 initially contacts the microtubule. It follows that molecules that solely diffuse along or stick to the microtubule without any processive behavior initially bind to the microtubule through their dynactin p150 subunit, and their dynein is in either an inhibited or otherwise inactive state.

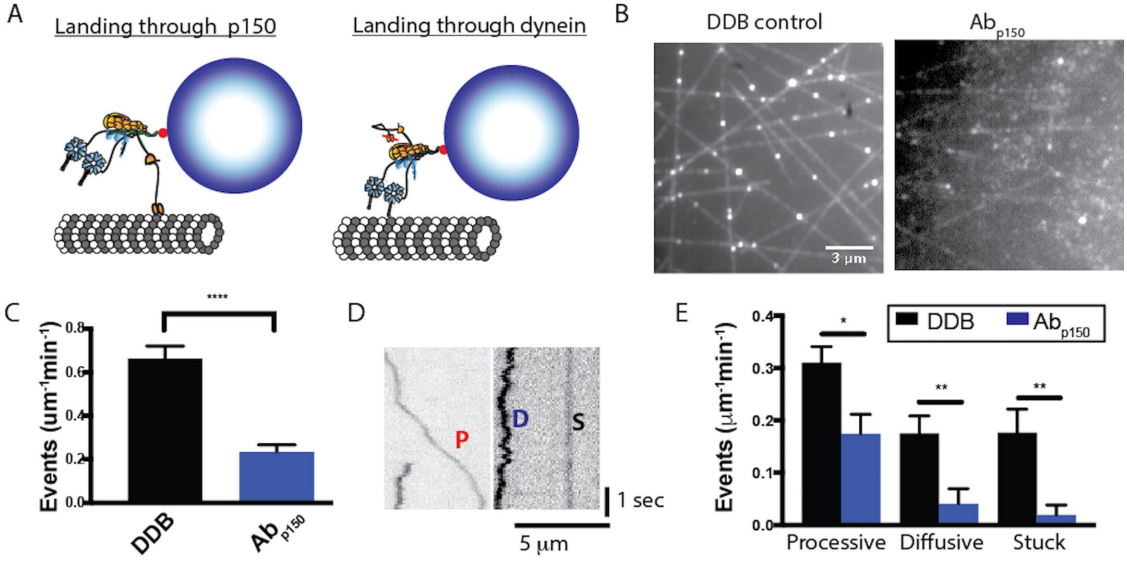

FIGURE 2: p150 of dynactin promotes landing of DDB complexes. (A) Diagram of landing experiment in the presence of ATP. Initial landing of Qdot-labeled DDB complexes on microtubules can occur either through dynein or through dynactin p150. (B) Field of microtubules and attached DDB complexes for control (left) and in the presence of Ab_{p150} (right). (C) Frequency of landing events in control (black, $n = 10$ microtubules in 50 s video length) and Ab_{p150} (blue, $n = 10$ microtubules in 50 s video length). Error bars are SEM; ****, $p < 0.001$ by two-tailed t test. (D) Kymographs of DDB landing events, showing processive (P), diffusive (D), and stuck (S) events. (E) Frequency of processive, diffusive, and stuck landing events for control DDB ($n = 10$ microtubules in 50 s) and DDB in the presence of Ab_{p150} ($n = 10$ microtubules in 50 s). Error bars are SEM; *, $p < 0.05$ and **, $p < 0.01$ by two-tailed t test.

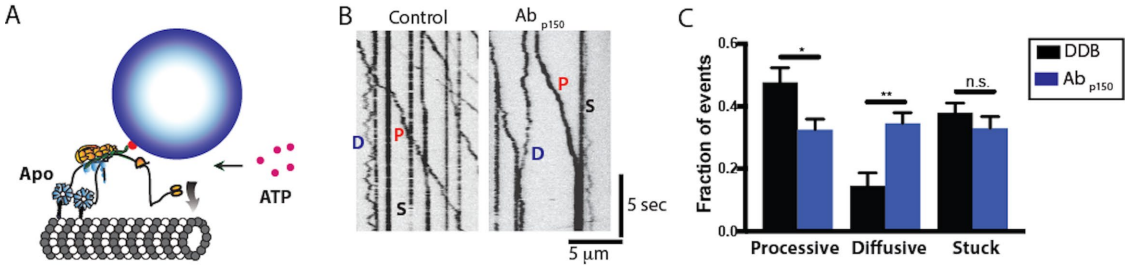

FIGURE 3: Blocking p150 dynactin leads to fewer processive events and more diffusive events following release from Apo-lock. (A) Diagram of the Apo-lock experiment. DDB complexes bind to immobilized microtubules in absence of ATP, and ATP buffer is flushed into the system to initiate motility. (B) Kymograph of DDB motility 5 min after flowing in ATP buffer for control (left) and in the presence of Ab_{p150} (right). Processive (P), diffusive (D), and stuck (S) events are noted. (C) Average fraction of processive, diffusive, and stuck traces across $n = 10$ kymographs for control (black) and $n = 10$ Ab_{p150} group (blue). Error bars are SEM; ** denotes $p < 0.01$; * denotes $p < 0.05$ (two-tailed t test); n.s., not significantly different.

Dynactin p150 enhances processive and diminishes diffusive behavior of DDB

To select for active DDB complexes, we introduced DDB into the chamber in the absence of ATP, such that active dynein bound to the immobilized microtubules in the apo (no nucleotide) state. Following this "Apo-lock," any unbound complexes were washed out with nucleotide-free buffer, and movement was initiated by flowing ATP-containing buffer into the chamber (Figure 3A). Here "active DDB complexes" are defined as those that bind microtubules statically in the apo state and release in the ATP state. As with the landing experiments, processive, diffusive, and stuck behaviors were all observed (Figure 3B). In the absence of dynactin p150 antibody, roughly half of the complexes moved processively upon ATP addition, whereas the other half either remained stuck in ATP (~40%) or displayed only diffusive behavior (~10%; Figure 3C; DDB). In the presence of dynactin p150 antibody, the fraction of processive complexes fell, while the fraction of diffusive complexes increased (Figure 3C; p150). This is the opposite of what would be predicted if p150 were simply acting as a diffusional tether; if that were the case, there should be fewer diffusive complexes when p150 is blocked. Although informative, this analysis categorized every particle as processive, diffusive, or stuck, which is relatively coarse. Deeper understanding of how dynein is activated in the DDB complex and how dynactin to p150 contributes this activation requires a more detailed analysis of the processive complexes, where DDB switches between processive, diffusive, and stuck states within a single run.

p150 promotes switching into and prevents switching out of the processive state

To investigate how p150 affects the kinetics of DDB switching between different motility states, we enhanced our temporal resolution by attaching 30-nm gold nanoparticles to BicD2 in our DDB complex and tracking them with interferometric scattering (iSCAT) microscopy. An iSCAT image is formed by interference between light scattered by the gold particle and light reflected at the glass–water interface of the sample (Figure 4A; Ortega-Arroyo and Kukura, 2012). With this approach, unlabeled microtubules and gold particles can be visualized simultaneously, with particles appearing as dark spots on a bright background (Figure 4B). After subtracting an image of the stationary microtubule and inverting the image to produce a bright particle on a dark background, the point-spread function of the gold particle can be fitted by a 2D Gaussian distribution (Figure 4D) to achieve nanometer-scale spatial precision. By analyzing movies with FIESTA software (Ruhnow *et al.*, 2011), *x*–*y* position over time data were collected at 100 frames/s, which we found to be the optimal temporal resolution for this work.

By processing the traces to obtain linear distance along the microtubule over time, DDB complexes clearly switch between processive, diffusive, and stuck states during a given trace (Figure 4E). Although some phases such as long processive or stuck phases are readily identifiable, diffusive phases are particularly difficult to define, despite the high spatiotemporal resolution. Thus, we developed an objective algorithm for classifying processive, diffusive, and stuck durations within a single trace. The algorithm, described fully in the Supplemental Information and in Supplemental Figures S2–S6, uses a 10-frame running window and calculates the positional SD, the slope, and the residual around the slope for each point in the trace. Based on defined cutoff values that are optimized with simulations, each point is classified and the traces are then broken into continuous segments of at least 100 msec (10 frames) duration each. A gallery of processed traces is shown in Figure 5, with colors indicating processive (red), diffusive (blue), and stuck (black) states.

Dividing each single-molecule trajectory into different phases, or motility states, provides distributions of time the motor spends in each state, as well as the switching rates between the three states. For DDB under control conditions, processive segments had the longest duration at 0.81 s, followed by stuck (0.53 s) and diffusive (0.23 s) phases (Figure 6A). The most frequent switching was between stuck and processive states (Figure 6A, inset), meaning that there were relatively frequent short pauses during processive stepping. The second most common switching was between processive and diffusive states. These two behaviors can be seen qualitatively in Figure 5 as short black and blue phases interspersed in the relatively long processive runs in red.

From the state durations and switching frequencies, we created a kinetic model for how DDB switches between processive, diffusive, and stuck states and what fraction of the time the motors spend in each state. Each state (P, D, and S) has two transitions in and two transitions out, and all transitions were assumed to be first order based on the roughly exponential distribution profiles in Figure 6A. The transition rate out of any given state equals the sum of the two rate constants exiting that state, and the relative rates between the two exit paths are taken from the measured switch rates in Figure 6A, inset. The switching model (Figure 6B) provides a wealth of information. First, the motors spend 65% of the time in the processive state and most of the remaining time (31%) in the stuck (paused) state. Second, if the motors ever enter the diffusive state or the stuck state, they rapidly transition back to the processive state (at 3.9 and 1.8 s^{-1}, respectively). Finally, transient events that break up

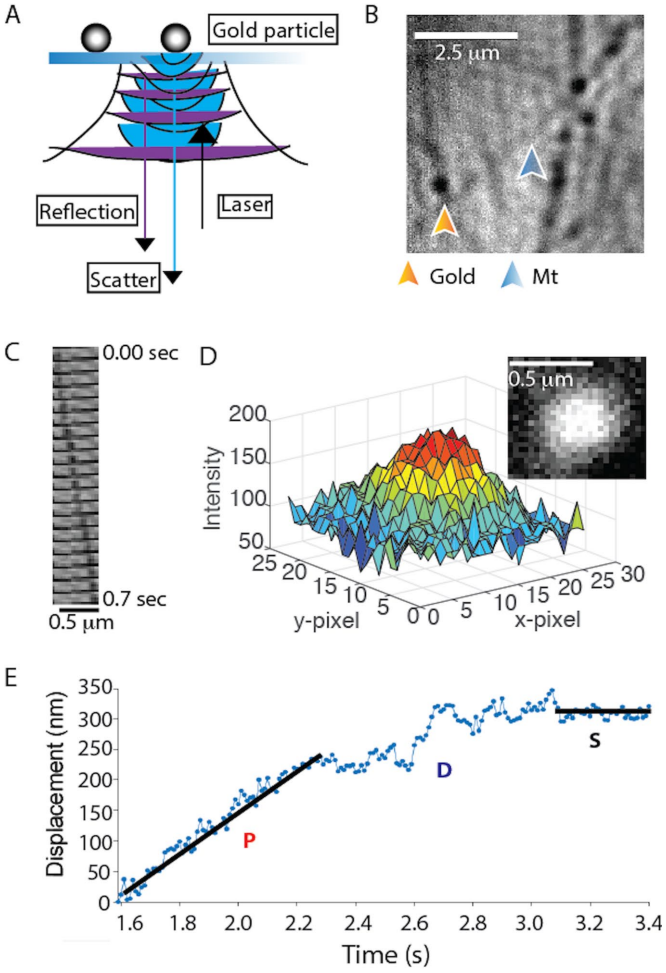

FIGURE 4: Single-molecule DDB tracking by iSCAT microscopy. (A) Diagram of iSCAT microscopy. Image is formed by scattered light from the gold nanoparticle (blue) interfering with reflected light from the glass–water interface (purple). (B) iSCAT image of a field of gold nanoparticle–labeled DDB bound to surface-immobilized microtubules. Image shown is generated from a raw image by flat fielding, which corrects inhomogeneous illumination across the field. (C) Montage of a gold particle–labeled DDB moving along an immobilized microtubule; each image is 35 msec apart. (D) Plot of pixel intensity of a gold nanoparticle (image in inset), which is fitted by a 2D Gaussian for subpixel localization. Image is generated by subtracting the image of the stationary microtubule (taken later in the video when no gold-labeled motor is present) and inverting the image to obtain a bright particle on a dark background. See also Supplemental Video S1. (E) Distance vs. time trace of a single DDB, demonstrating processive (P), diffusive (D), and stuck (S) episodes in the same trace. Lines represent linear regressions to hand-selected segments.

the processive runs are more often short pauses (occurring at a frequency of 1 s^{-1}), rather than diffusive episodes (at a frequency of 0.23 s^{-1}).

To understand the role of dynactin p150 in dynein activation and diffusional tethering, we repeated the analysis for DDB in the presence of the p150 antibody. When dynactin p150 was blocked, the duration of the processive segments decreased to 0.61 s, while the duration of diffusional segments increased to 0.37 s (Figure 6C). Compared to control, switching occurred less frequently between processive and stuck states, and more frequently between processive and diffusive states (Figure 6C, inset). As clearly shown in the kinetic model (Figure 6D), blocking p150 caused the motor to spend less time in the processive state (55%) and more time in the diffusive state (16%). The kinetic explanation for this (highlighted by red and blue arrows in Figure 6, B and D; see also Supplemental Figure S9) is that the presence of p150 causes DDB to switch 69% *more* frequently from the diffusive state into the processive state and to switch 73% *less* frequently out of the processive state back to the diffusive state. To summarize, allowing p150 to interact with the microtubule both promotes and stabilizes the processive state of dynein in the DDB complex.

To investigate whether p150 directly interacts with microtubules in motile DDB complexes, we first compared the mean velocities of processive segments in the absence and presence of the p150 antibody. The algorithm-identified processive segments showed a broad velocity distribution (Supplemental Figure S7); this is consistent with published work (McKenney *et al.*, 2014; Tripathy *et al.*, 2014; Belyy *et al.*, 2017; Gutierrez *et al.*, 2017) and its source is not understood. Importantly, blocking p150 did not increase the mean velocity (control: V = 328 ± 28 nm/s; Ab_{p150}: V = 340 ± 22 nm/s; n.s., $p = 0.72$ using a two-tailed *t* test; Supplemental Figure S7), arguing that p150 does not act as a brake slowing dynein in the DDB complex. We next asked whether the diffusive episodes in the control and p150 antibody cases represented similar structural states, by calculating the diffusion constant for diffusive segments from the two groups. The diffusion constants were similar (control: D = 16,000 ± 4100 nm^2/s; Ab_{p150}: D = 17,000 ± 1300 nm^2/s; Supplemental Figure S8), which is roughly fourfold slower than the value reported for isolated p150 (Tripathy *et al.*, 2014). Thus, the data are consistent with the diffusive states being due to dynein rather than p150 interacting with the microtubule.

p150 enhances minus-end directionality of kinesin–DDB complexes

Based on the finding that p150 enhances the time DDB spends in the processive state, it follows that p150 should enhance dynein's ability to compete against kinesin-1 in a tug-of-war such as occurs during intracellular bidirectional transport. To investigate this possibility, we reconstituted the kinesin–dynein bidirectional transport system in vitro using a DNA origami scaffold. One kinesin-1 motor and one DDB were connected through a DNA scaffold functionalized with a quantum dot (Figure 7A), and the complexes tracked by TIRF microscopy. Consistent with previous in vitro tug-of-war experiments (Belyy *et al.*, 2017), long duration events were observed with mean velocities much slower than either individual unloaded motor speed, indicating that both motors engaged with the microtubule (Figure 7B). To investigate the role of p150 in bidirectional transport, we compared the mean velocities of traces in the absence and presence of Ab_{p150}. The simple prediction is that, if blocking p150 increases the fraction of time the motor is in the diffusive state (from 4% to 16%; Figure 6, B and D), then the mean velocity should shift toward the plus end in the presence of the antibody. For the control case, we measured a mean velocity of –9.1 ± 9.2 nm/s (mean ± SEM, $n = 33$) toward the minus end (Figure 7D). In the presence of Ab_{p150}, the mean velocity shifted to 62 ± 17 nm/s (mean ± SEM, $n = 32$; Figure 7D), a statistically significant change ($p = 0.0004$ by a two-tailed *t* test). In addition, the proportion of complexes with a net plus-end directionality increased from 42% in the control case to 75% when p150 was blocked (Figure 7E).

The +71 ± 19 nm/s shift in the mean velocity when p150 was blocked is in good quantitative agreement with our switching model, as follows. The diffusive episodes had a 1D diffusion

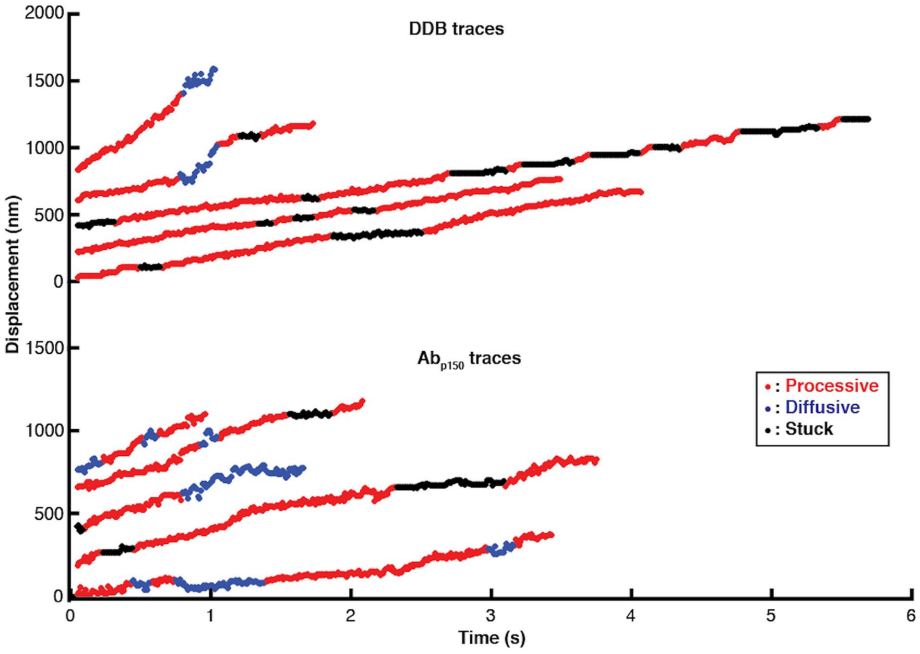

FIGURE 5: High-resolution DDB tracking and motility state identification. Sample traces of control DDB (top) and DDB in the presence of Ab_{p150} (bottom) taken at 100 frames/s by iSCAT microscopy and processed with the state switching algorithm. Processive segments are labeled in red, diffusive episodes in blue, and stuck durations in black.

constant of D = 16,000 nm^2/s by mean-squared displacement analysis (Supplemental Figure S8). This can be converted to a drag coefficient, γ, using $D = k_BT/\gamma$, where Boltzmann's constant times absolute temperature, k_BT = 4.1 pN nm (Howard, 2001). The resulting drag coefficient of γ = 0.0002 pN s/nm means that a DDB in the diffusive state that is being pulled by a kinesin moving at v = 600 nm/s should produce a drag force ($F = \gamma * v$) of only 0.1 pN, which should not slow the kinesin (Schnitzer *et al.*, 2000). From the switching model in Figure 6, B and D, blocking p150 increased the fraction of time in the diffusive state by 12%, from 4% to 16%. If the complexes move at 600 nm/s (Mickolajczyk and Hancock, 2017) for 12% of the time, this would contribute 0.12 * 600 nm/s = 72 nm/s of mean plus-end velocity, which closely matches the observed +71 ± 19 nm/s increase (Figure 7F). Thus, we interpret the slow kinesin–DDB transport velocities to reflect the antagonistic motors pulling against one another with DDB stochastically switching between motile states. Blocking p150 shifts DDB toward more time in the diffusive state that kinesin readily pulls against, resulting in a plus-end shift in the net transport velocity.

DISCUSSION

Understanding how specific intracellular cargoes are targeted to their proper cellular locations requires understanding how bidirectional transport is regulated, which in turn requires understanding the regulation of dynein activation. By tracking DDB complexes at high temporal resolution and applying our change-point detection algorithm, we found that in the DDB complex, dynein switches between active and inactive states at rates exceeding 1 s^{-1} (Figure 6B). This analysis leads to two questions. First, to what degree is dynactin p150 tethering the complex during processive motility? Second, do the diffusive and stuck periods reflect only p150 interacting with the microtubule, only inhibited dynein interacting with the microtubule, or some combination of the two? Blocking p150 provides the following insights. First, the observation that blocking p150 results in more, rather than fewer diffusive complexes (Figure 3C) suggests that diffusive DDB behavior, also observed by others (McKenney *et al.*, 2014, 2016; Schlager *et al.*, 2014; Cianfrocco *et al.*, 2015), reflects complexes where dynein is in an inhibited state that binds to microtubules, rather than complexes that are tethered solely through p150. Second, the longer durations of diffusive segments following p150 block (Figure 6C) suggests that switching into this state during processive runs reflects dynein switching into an inhibited state, rather than dynein detaching from the microtubule while p150 maintains overall microtubule association of the complex. Third, the finding that the switching rate into and out of the stuck state during processive runs was unaffected by Ab_{p150} (Figure 6, B and D) suggests that this paused state is inherent to the stepping mechanism of dynein or at least that p150 alone is not sufficient to prevent the formation of this inhibited state. And last, there was no significant difference between mean velocities of processive segments in control versus p150 block (Supplemental Figure S7), arguing that p150 does not act as a brake slowing dynein in the DDB complex.

Previous work in the absence of BicD2 showed that 1) isolated p150 subunits diffuse on microtubules, 2) isolated p150 and dynactin both enhance dynein processivity, and 3) deleting the CAP-Gly domain of p150 increased dynein velocity (King and Schroer, 2000; Ayloo *et al.*, 2014). These results seem in conflict with our observation that blocking p150 increased the diffusional behavior of DDB and had no effect on the velocity. However, p150 appears to play a different role on its own than it does in the presence of dynein activators, and previous work on DDB complexes in fact supports our work. McKenney *et al.* (2016) found that deleting the C-terminal tail (CTT) or terminal tyrosine of α-tubulin almost completely abolished microtubule binding of isolated p150, consistent with the established interaction between the CAP-Gly domain and the tubulin CTT. However, on segmented microtubules, processively moving DDB complexes successfully traversed detyrosinated or CTT-deleted segments without interruption, suggesting that p150-microtubule tethering is not required for motility (McKenney *et al.*, 2016). In related work, tau condensates were shown to block initial DDB binding and to form a barrier that blocked the diffusion of isolated p150, but processive DDB successfully traversed the condensates (Tan *et al.*, 2019). Thus, previous work established a clear role for p150 in the initial binding of DDB to microtubules, which we also found, but did not clearly establish a tethering role for p150 in processively moving DDB complexes. Our work expands this picture by finding transient diffusive phases that interrupt processive runs of DDB represent inactive dynein, rather than p150 diffusively tethering the DDB complexes to microtubules.

On the basis of recent structural studies, we can make tentative structural assignments to our identified functional states of dynein. Because the dynein–dynactin–BicD2 structure is

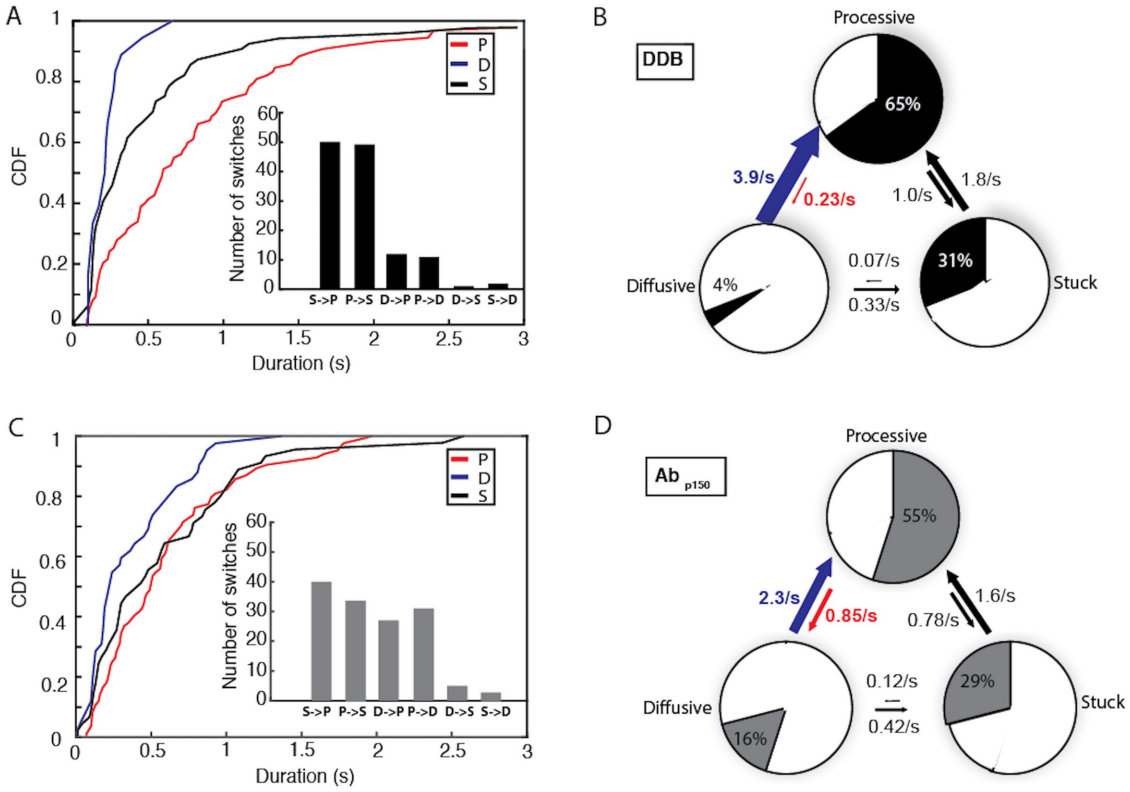

FIGURE 6: p150 shortens diffusive segments and elongates processive segments. (A) Cumulative distributions of processive, diffusive, and stuck segment durations for control DDB. Mean durations were 0.81 s for processive, 0.23 s for diffusive, and 0.53 s for stuck states. Inset: Number of detected state switches over 93 s total analyzed time from 31 molecules. (B) State switching diagram showing first-order switching rates between states and the fraction of time spent in each state for control DDB. The blue arrow denotes the most significant decrease in switching rate with Ab_{p150}, while the red arrow denotes the most significant increase in switching rate. (C) Cumulative distributions of processive, diffusive, and stuck segment durations for DDB in the presence of Ab_{p150}. Mean durations were 0.61 s for processive, 0.37 s for diffusive, and 0.60 s for stuck states. Inset: number of detected state switches for the Ab_{p150} group over 100 s total analyzed time from 32 molecules. (D) State switching diagram showing first-order switching rates between states and the fraction of time spent in each state DDB in the presence of Ab_{p150}.

incompatible with dynein being in the inhibited "phi" state (Zhang *et al.*, 2017), we interpret our DDB complexes to reflect dynein in the "open" conformation, with the heads either in an "open-parallel" configuration optimal for stepping, or an "open-inverted" conformation that can bind to microtubules but not processively step (Figure 8A; Zhang *et al.*, 2017). Dynein diffusion in the open-inverted state could either be through the action of one diffusive head or result from the molecule flipping 180° and the two microtubule binding domains alternately binding. Similarly, we hypothesize that in the DDB structure, p150 is sterically free and able to reversibly interact with microtubules (Urnavicius *et al.*, 2015). This leads to four possible states (Figure 8A), with dynein being in either an open-parallel or open-inverted conformation and p150 either interacting with the microtubule and constraining the dynactin orientation, or p150 being free and dynactin being less conformationally constrained. In this model, when p150 interacts with the microtubule, the open-parallel conformation of dynein is favored, whereas blocking p150 from binding to the microtubule biases the motor toward the open-inverted conformation (highlighted states in Figure 8A).

Instead of predominantly acting as a diffusive tether in the DDB complex, our data support a model in which p150 is an allosteric activator of dynein. This allosteric mechanism in DDB differs from one proposed previously based on the effects of isolated p150 CC1 fragments lacking the CAP-Gly domain on the motility of isolated dynein (Tripathy *et al.*, 2014). The clearest evidence for this allosteric activation in DDB is the faster switching into the processive state and slower switching out of the processive state in the control compared with the p150 block (Figure 6, B and D, and Supplemental Figure S9). Assuming that the action of p150 is through binding to the microtubule rather than binding to the dynein heads, how could this work? Recent studies investigating the regulatory protein Lis1 and adapters like BicDR and Hook3 that can form complexes containing two dyneins have converged on a model in which a second dynein (or even the linker and tail of a second dynein) enhances motility by stabilizing the first dynein in the open-parallel state (Zhang *et al.*, 2017; Urnavicius *et al.*, 2018; Elshenawy *et al.*, 2019; Htet *et al.*, 2019). Based on this, a possible explanation for p150 enhancement of motility is that when p150 is tethered to the microtubule, it orients the dynactin filament, and hence the dynein heads, in a conformation that favors the open-parallel conformation (Figure 8A). Conversely, if p150 does not stabilize dynactin on the microtubule, the dynactin filament and the two dynein heads are free to adopt multiple conformations including the nonmotile open-inverted state that either diffuses along or sticks to microtubules.

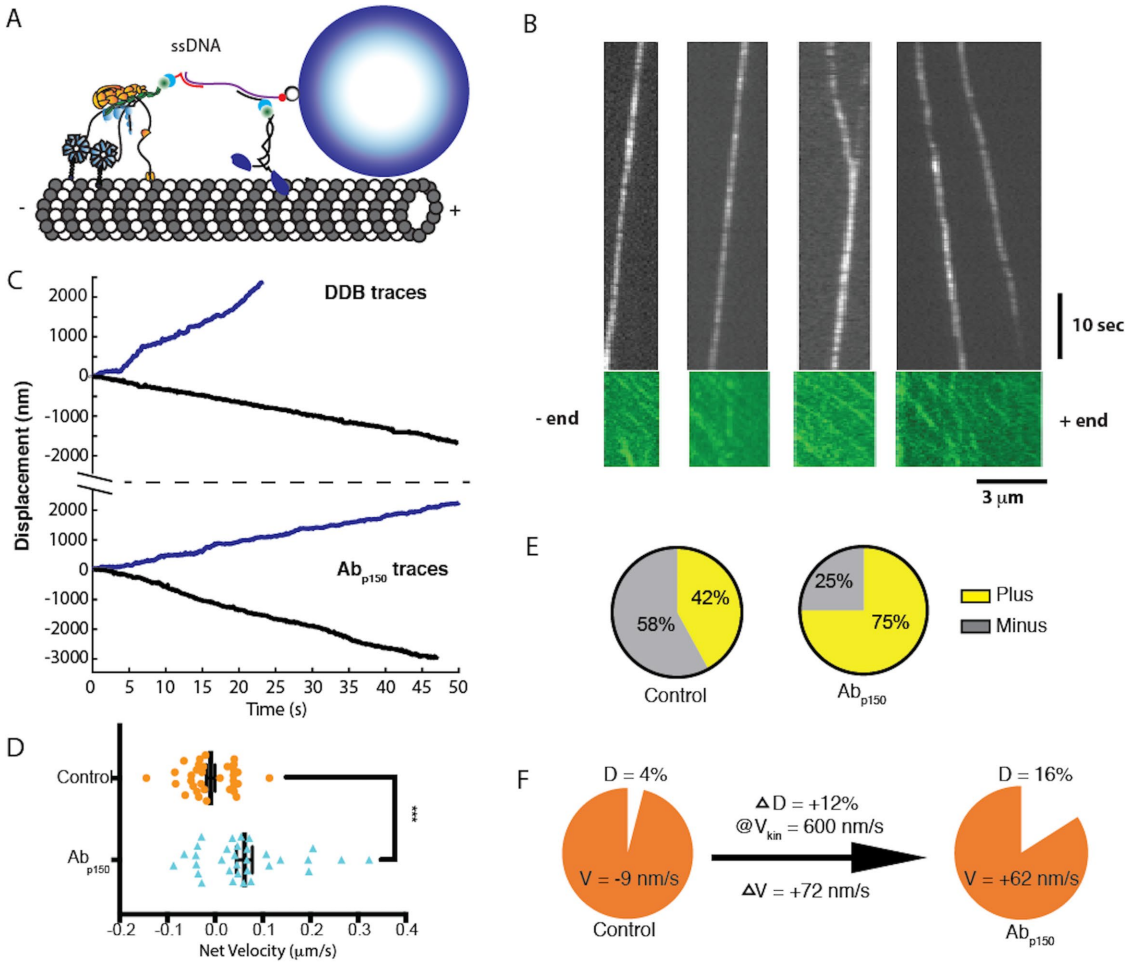

FIGURE 7: p150 activates DDB in kinesin–DDB bidirectional transport. (A) Diagram of the reconstituted bidirectional transport system. Single kinesin-1 and DDB are connected through single-stranded DNA-functionalized GBP1 and GBP2 adapters to a double-stranded DNA scaffold, linked at its biotinylated 5′ end to a streptavidin-coated Qdot. (B) Kymographs Qdot-labeled DDB–kinesin-1 (top) in the 647 nm channel, and the excess kinesin-1 motors streaming to the plus end in the GFP channel (bottom), used to identify the polarity of the microtubule. See also Supplemental Video S2. (C) Sample traces of DDB–kinesin-1 for control (top) and the Ab$_{p150}$ group (bottom). (D) Velocities of the control group (orange; –9.1 ± 9.2 nm/s; mean ± SEM, n = 33) and the Ab$_{p150}$ group (blue: 62 ± 17 nm/s; mean ± SEM, n = 32) calculated from linear regression to entire traces. The two groups were significantly different by two-tailed t test, ***, p < 0.0005. (E) Percent of plus-end directed cargoes (yellow) and minus-end directed cargoes (gray) for the control kinesin–DDB group (left) and the Ab$_{p150}$ group (right). (F) Graphical explanation of velocity shift. Blocking p150 increased the fraction of time in the diffusive state by 12%. If it is assumed that the complexes move at the unloaded kinesin-1 velocity during this time, then the expected shift in mean velocity is 0.12 * 600 nm/s = 72 nm/s toward the plus end, in agreement with measurements.

In contrast to the rapid switching behavior of isolated DDB, kinesin-DDB complexes displayed long duration events having slow mean velocities and both plus- and minus-end net directionalities. Work by others has also shown that adapters that more fully activate dynein generate a greater net minus-end directionality in kinesin–dynein complexes (Belyy *et al.*, 2017; Elshenawy *et al.*, 2019). Because kinesin acts as an effective tether to maintain association with the microtubule in kinesin–DDB complexes, p150 is not expected to play a tethering role. However, the significant plus-end velocity shift seen upon p150 inhibition demonstrates that p150 plays an activating role even when dynein is subjected to plus-end forces from kinesin-1. The fact that the +71 ± 19 nm/s shift in average speed upon p150 inhibition can be quantitatively explained by the 12% shift of DDB into the diffusive state (Figure 7F) is consistent with these kinesin–DDB pairs competing in a simple tug-of-war process in vitro. These data suggest that p150 can modulate bidirectional transport in cells by enhancing dynein motility and making it a stronger opponent to kinesin-1.

Whereas kinesins achieve functional diversity through gene duplication, there is only one cytoplasmic dynein heavy chain in the genome; thus, regulation of dynein motor properties and cargo interactions must be achieved through diversity in cargo adapters and exogenous regulatory proteins (Reck-Peterson *et al.*, 2018). Understanding dynein activation is important because during bidirectional cargo transport in cells, any regulation of dynein will alter its competition with kinesin, and hence affect cargo speed and directionality. By applying single-molecule iSCAT tracking with our novel switch-point detection algorithm, we identify switches between active and inhibited motor states in DDB and show that p150 affects the switching rates between these states. Thus, in addition to acting as a diffusional tether that can enhance dynein run lengths, p150 can enhance dynein stepping both in isolated

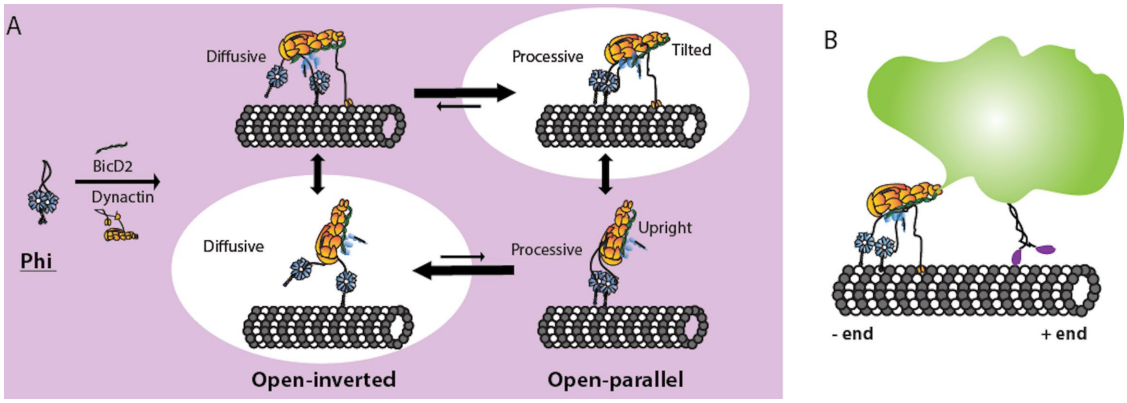

FIGURE 8: Proposed model for DDB motility enhancement by p150 dynactin. (A) Dynein can reside in the inactive phi conformation in solution, but forming a DDB complex results in dynein switching to an open conformation (Zhang *et al.*, 2017). In the open-inverted conformation, DDB is more likely to diffuse along microtubules, while in the open-parallel conformation DDB is more processive. Top, p150 interaction with the microtubule promotes a tilted dynactin geometry that stabilizes the open-parallel conformation of dynein and results in enhanced processivity. Bottom, blocking p150 causes dynactin to adopt a more flexible upright geometry that promotes the open-inverted conformation of dynein and results in DDB diffusing on the microtubule. Thus, complexing with BicD2 and dynactin activates dynein by inhibiting the phi conformation, and interaction of p150 further activates dynein by stabilizing the open-parallel conformation of the two dynein heads. (B) Implications for bidirectional cargo transport in cells: enhancement of DDB processivity by p150 promotes net minus-end cargo transport.

DDB complexes and in antagonistic assemblies of DDB and kinesin-1, and as such should be added to the list of dynein-activating proteins.

MATERIALS AND METHODS

Plasmid constructs and DDB purification

Mouse BicD2 (25–400 aa; McKenney *et al.*, 2014) was inserted into the pET28a plasmid with an N-term StrepII tag and a C-term eGFP and His6 tag, expressed in *Escherichia coli*, and purified by Ni column chromatography. Bovine brains were sliced and flash-frozen on dry ice at the slaughterhouse, and stored at −80°C. To purify DDB, brain was mixed with an equal volume of 50H50P buffer (50 mM HEPES, 50 mM PIPES, 2 mM $MgSO_4$, 1 mM EDTA, pH 7.0), incubated in a 37°C water bath, and then homogenized in a blender, following published protocols (McKenney *et al.*, 2014). The lysate was clarified by centrifugation at 30,000 × *g* for 30 min, and the supernatant was mixed with equal volume A buffer (30 mM HEPES, 1 mM EGTA, 50 mM K-acetate, 2 mM Mg-acetate, 10% glycerol, pH 7.4) supplemented with 3 mM dithiothreitol (DTT), 1 mM phenylmethylsulfonyl fluoride, and 0.1% NP-40 alternative (McKenney *et al.*, 2014). The mixture was further centrifuged at 100,000 × *g* for 20 min, and the supernatant mixed with 100 nM BicD2 and incubated at 4°C for 2 h. A column containing 2 ml of Strep-Tactin beads (IBA, Lifesciences) was rinsed with three column volumes of A buffer, the sample was applied to the column, the column was washed with A buffer, and the protein was eluted with A buffer containing 3 mM DTT and 5 mM D-Desthiobiotin (Sigma-Aldrich). The eluted DDB was used directly in single-molecule experiments or flash-frozen on liquid N_2 and stored at −80°C.

Nanoparticle functionalization of DDB

DDB containing a C-terminal GFP was attached to streptavidin-functionalized nanoparticles through a biotinylated GBP nanobody (Kubala *et al.*, 2010; Feng *et al.*, 2018). Following a previous approach (Mickolajczyk *et al.*, 2015), a coexpression plasmid containing the BirA enzyme was constructed by inserting the GBP (Feng *et al.*, 2018) sequence followed by a C-terminal Avi-tag (GLNDIFEAQKIEWH; Mickolajczyk *et al.*, 2015) and His_6 tag. Biotinylated GBP was bacterially expressed and purified by Ni column chromatography. Flow cells were constructed using coverslips washed three times each with 70% ethanol and ddH_2O. Taxol-stabilized, Cy5-labeled bovine brain microtubules (10% labeling) were absorbed onto the coverslips using full-length rigor kinesin, as previously described (Shastry and Hancock, 2011; Mickolajczyk *et al.*, 2015). Motility buffer was based on A buffer and consisted of 30 mM HEPES, 1 mM ethylene glycol tetraacetic acid (EGTA), 50 mM K-acetate, 2 mM Mg-acetate, 10% glycerol, 10 μM Taxol, 0.2 mg/ml casein, 0.02 mg/ml glucose oxidase, 20 mM D-glucose, 0.008 mg/ml catalase, and 1 mM ATP, pH 7.4. For landing experiments, a 1:1 mixture of DDB complexes and GBP were incubated together for 5 min, the solution diluted to 10 nM with motility buffer, mixed with 10 nM streptavidin-coated quantum dots (655 nm emission; Life Technologies), and incubated for 5 min. The final DDB–Qdot mixture was then added to the flow cell in the presence of 1 mM ATP and visualized. In Apo-lock experiments, 10 nM DDB complexes (based on GFP fluorescence) were first added to the flow cell in the absence of ATP and incubated for 5 min to allow binding to the microtubules. After a wash with buffer B (30 mM HEPES, 1 mM EGTA, 50 mM K-acetate, 2 mM Mg-acetate, 10% glycerol, 10 μM Taxol, 0.2 mg/ml casein, pH 7.4) to remove unbound complexes, a 10 nM solution of GBP diluted in buffer B was injected and incubated for 5 min to allow binding to BicD-GFP. Next, 10 nM streptavidin-coated quantum dots diluted in buffer B were injected into the flow cell, and allowed 5 min to bind to the biotinylated GBP. Finally, a motility buffer containing 1 mM ATP was injected to initiate motility, and the flow cell was transferred to the microscope.

Fluorescence microscopy and particle tracking

Single-molecule quantum dot experiments were carried out by TIRF microscopy, as previously described (Feng *et al.*, 2018). For each field, an image was taken of the Cy5-labeled microtubules, and then 500-frame movies were taken at 20 frames/s, starting 5 min after injecting the final motility buffer. Movies were taken from at least

five independent flow cells for each measurement. Antibody experiments used Ab_{p150} (BD, Biosciences; No. 610474; King and Schroer, 2000; Payne *et al.*, 2003; Ross *et al.*, 2006; Dixit *et al.*, 2008; Ayloo *et al.*, 2014), which was previously used to block interactions of dynactin p150 with microtubules (King and Schroer, 2000; Ross *et al.*, 2006). DDB was mixed with 25 µg/ml Ab_{p150}, incubated on ice for 30 min to allow binding, and then introduced into the flow cell, with all subsequent solutions introduced into the flow cell also containing 25 µg/ml Ab_{p150}. Image processing and kymograph analysis were performed in ImageJ (National Institutes of Health, Bethesda, MD). Landing rates were calculated by counting all events on a given microtubule for a 10-s video length, and normalizing the counts to per min per microtubule length. The minimum event duration was 200 ms.

ISCAT microscopy and image processing

Flow cells for iSCAT microscopy were prepared similarly to TIRFM, with minor modifications. After Apo-lock of DDB to microtubules, 1 nM GBP in buffer B was introduced and incubated for 5 min, followed by 1 nM of 30-nm gold nanoparticles (BBI Solutions) in buffer B and a 5 min incubation to allow binding. Finally, a motility buffer containing 1 mM ATP was introduced and incubated for 5 min to initiate movement, and the flow cell transferred to the microscope. The iSCAT microscope used in the work was described previously (Mickolajczyk *et al.*, 2019). Images were taken using custom written LabVIEW software. The videos were taken at 100 frames/s for 1000 frames with an effective pixel size of 32 nm. Even illumination was achieved through flat fielding before image acquisition (Mickolajczyk *et al.*, 2015). A background image of stationary microtubules before or after particle binding was subtracted from the stack of iSCAT images, and the resulting movies were then inverted to obtain a bright gold signal on a dark background. Particle positions over time were tracked by FIESTA (Ruhnow *et al.*, 2011); if no particle position was determined for 10 consecutive frames due to low signal/noise, the trace was terminated. Details for the switch detection algorithm are provided in the Supplemental Information.

Kinesin-1/DDB origami experiments

DDB and *Drosophila* kinesin-1 motors (truncated at residue 560 and C-terminal GFP tagged; Shastry and Hancock, 2011) were linked to a double-stranded DNA scaffold following a previously published protocol employing GBP functionalized with specific single-stranded DNA (Feng *et al.*, 2018). To generate motors functionalized with different oligonucleotides, DDB was incubated for 15 min on ice with GBP1 in excess, and kinesin incubated with GBP2 in excess in buffer B. Next, DDB-GBP1 was incubated for 15 min on ice with an excess concentration of DNA scaffold containing single-stranded overhangs on both ends and biotin on one end (Figure 7A; scaffold described previously; Feng *et al.*, 2018). The mixture was then introduced into a flow cell containing surface-immobilized microtubules, and incubated for 5 min in the absence of ATP to allow binding of the DDB–GBP1–DNA complexes to the microtubules. The flow cell was then washed twice with buffer B to remove any unbound motors, BicD2, and GBP1, leaving only DDB with attached DNA scaffolds bound to the microtubules. An excess of kinesin-1–GBP2 was then introduced into the flow cell and incubated for 5 min to populate the second end of the DNA scaffolds with kinesin motors. Quantum dots (1 nM, 655 nm emission) were then introduced into to the flow cell in motility buffer containing 1 mM ATP to label the DNA scaffolds and initiate movement, and videos were taken immediately. To determine microtubule polarity, we observed the plus-end streaming of the free GFP-labeled kinesin-1 motors in the GFP channel (Figure 7B and Supplemental Video S2).

Data and code

Data and code are available to readers in the Pennsylvania State University institutional repository, ScholarSphere, https://doi.org/10.26207/ap7j-3b07.

ACKNOWLEDGMENTS

We thank Richard J. McKenney for generously providing the BicD2 plasmid and advice on DDB purification, Geng-Yuan Chen for assistance with the switch-point detection algorithm, Keith J. Mickolajczyk for iSCAT microscopy mentoring, and members of the W.O.H. laboratory for helpful discussions. This work was supported by National Institutes of Health Grants no. R01GM-121679 and no. R01GM-122082 to W.O.H.

REFERENCES

Ayloo S, Lazarus JE, Dodda A, Tokito M, Ostap EM, Holzbaur ELF (2014). Dynactin functions as both a dynamic tether and brake during dynein-driven motility. Nat Commun 5, 1–11.

Belyy V, Schlager MA, Foster H, Reimer AE, Carter AP, Yildiz A, Avenue FC (2017). The mammalian dynein/dynactin complex is a strong opponent to kinesin in a tug-of-war competition. Nat Cell Biol 18, 1018–1024.

Cianfrocco MA, DeSantis ME, Leschziner AE, Reck-Peterson SL (2015). Mechanism and regulation of cytoplasmic dynein. Annu Rev Cell Dev Biol 31, 83–108.

Dixit R, Levy JR, Tokito M, Ligon LA, Holzbaur ELF (2008). Regulation of dynactin through the differential expression of p150 glued isoforms. J Biol Chem 283, 33611–33619.

Elshenawy MM, Kusakci E, Volz S, Baumbach J, Bullock SL, Yildiz A (2019). Lis1 activates dynein motility by pairing it with dynactin. BioRxiv 685826.

Feng Q, Mickolajczyk KJ, Chen GY, Hancock WO (2018). Motor reattachment kinetics play a dominant role in multimotor-driven cargo transport. Biophys J 114, 400–409.

Gross SP, Carolina Tuma M, Deacon SW, Serpinskaya AS, Reilein AR, Gelfand VI (2002). Interactions and regulation of molecular motors in *Xenopus* melanophores. J Cell Biol 156, 855–865.

Grotjahn DA, Chowdhury S, Xu Y, McKenney RJ, Schroer TA, Lander GC (2018). Cryo-electron tomography reveals that dynactin recruits a team of dyneins for processive motility. Nat Struct Mol Biol 25, 203–207.

Gutierrez PA, Ackermann BE, Vershinin M, Mckenney RJ (2017). Differential effects of the dynein-regulatory factor Lissencephaly-1 on processive dynein-dynactin motility. J Biol Chem 292, 12245–12255.

Hancock WO (2014). Bidirectional cargo transport: moving beyond tug of war. Nat Rev Mol Cell Biol 15, 615–628.

Hendricks AG, Perlson E, Ross JL, Schroeder HW, Tokito M, Holzbaur ELF (2010). Motor coordination via a tug-of-war mechanism drives bidirectional vesicle transport. Curr Biol, 20, 697–702.

Howard J (2001). Mechanics of Motor Proteins and the Cytoskeleton, Sunderland, MA: Sinauer Associates.

Htet ZM, Gillies JP, Baker RW, Leschziner AE (2019). Lis1 promotes the formation of maximally activated cytoplasmic dynein-1 complexes. BioRxiv 683052.

King SJ, Schroer TA (2000). Dynactin increases the processivity of the cytoplasmic dynein motor. Nat Cell Biol 2, 20–24.

Kubala MH, Kovtun O, Alexandrov K, Collins BM (2010). Structural and thermodynamic analysis of the GFP:GFP-nanobody complex. Protein Sci 19, 2389–2401.

Ligon LA, Tokito M, Finklestein JM, Grossman FE, Holzbaur ELF (2004). A direct interaction between cytoplasmic dynein and kinesin I may coordinate motor activity. J Biol Chem 279, 19201–19208.

Lloyd TE, Machamer J, O'Hara K, Kim JH, Collins SE, Wong MY, Sahin B, Imlach W, Yang Y, Levitan ES, *et al.* (2012). The p150Glued CAP-Gly domain regulates initiation of retrograde transport at synaptic termini. Neuron 74, 344–360.

McKenney RJ, Huynh W, Tanenbaum ME, Bhabha G, Vale RD (2014). Activation of cytoplasmic dynein motility by dynactin-cargo adapter complexes. Science 345, 337–341.

McKenney RJ, Huynh W, Vale RD, Sirajuddin M (2016). Tyrosination of α-tubulin controls the initiation of processive dynein–dynactin motility. EMBO J 35, 1175–1185.
Mickolajczyk KJ, Deffenbaugh NC, Arroyo JO, Andrecka J, Kukura P, Hancock WO (2015). Kinetics of nucleotide-dependent structural transitions in the kinesin-1 hydrolysis cycle. Proc Natl Acad Sci USA 112, 7186–7193.
Mickolajczyk KJ, Geyer EA, Kim T, Rice LM, Hancock WO (2019). Direct observation of individual tubulin dimers binding to growing microtubules. Proc Natl Acad Sci USA 116, 7314–7322.
Mickolajczyk KJ, Hancock WO (2017). Kinesin processivity is determined by a kinetic race from a vulnerable one-head-bound state. Biophys J 112, 2615–2623.
Monroy BY, Sawyer DL, Ackermann BE, Borden MM, Tan TC, Ori-McKenney KM (2018). Competition between microtubule-associated proteins directs motor transport. Nat Commun 9, 1–12.
Moughamian AJ, Holzbaur ELF (2012). Dynactin is required for transport initiation from the distal axon. Neuron, 74, 331–343.
Müller MJI, Klumpp S, Lipowsky R (2008). Tug-of-war as a cooperative mechanism for bidirectional cargo transport by molecular motors. Proc Natl Acad Sci USA 105, 4609–4614.
Nobutaka H, Shinsuke N, Yosuke T (2010). Molecular motors in neurons: transport mechanisms and roles in brain function, development, and disease. Neuron, 68, 610–638.
Olenick MA, Holzbaur ELF (2019). Dynein activators and adaptors at a glance. J Cell Sci 132, 1–7.
Olenick MA, Tokito M, Boczkowska M, Dominguez R, Holzbaur ELF (2016). Hook adaptors induce unidirectional processive motility by enhancing the dynein-dynactin interaction. J Biol Chem 291, 18239–18251.
Ortega-Arroyo J, Kukura P (2012). Interferometric scattering microscopy (iSCAT): new frontiers in ultrafast and ultrasensitive optical microscopy. Phys Chem Chem Phys 14, 15625–15636.
Payne C, St. John JC, Ramalho-Santos J, Schatten G (2003). LIS1 association with dynactin is required for nuclear motility and genomic union in the fertilized mammalian oocyte. Cell Motil Cytoskeleton 56, 245–251.
Reck-Peterson SL, Redwine WB, Vale RD, Carter AP (2018). The cytoplasmic dynein transport machinery and its many cargoes. Nat Rev Mol Cell Biol 19, 382–398.
Ross JL, Wallace K, Shuman H, Goldman YE, Holzbaur ELF (2006). Processive bidirectional motion of dynein–dynactin complexes in vitro. Nat Cell Biol 8, 562–570.
Ruhnow F, Zwicker D, Diez S (2011). Tracking single particles and elongated filaments with nanometer precision. Biophys J 100, 2820–2828.
Schlager MA, Hoang HT, Urnavicius L, Bullock SL, Carter AP (2014). In vitro reconstitution of a highly processive recombinant human dynein complex. EMBO J 33, 1855–1868.
Schnitzer MJ, Visscher K, Block SM (2000). Force production by single kinesin motors. Nat Cell Biol 2, 718–723.
Schroeder CM, Vale RD (2016). Assembly and activation of dynein–dynactin by the cargo adaptor protein Hook3. J Cell Biol 214, 309–318.
Shastry S, Hancock WO (2011). Interhead tension determines processivity across diverse N-terminal kinesins. Proc Natl Acad Sci USA 108, 16253–16258.
Sladewski TE, Billington N, Ali MY, Bookwalter CS, Lu H, Krementsova EB, Schroe TA, Trybus KM (2018). Recruitment of two dyneins to an mRNA-dependent bicaudal D transport complex. Elife 7, e36306.
Splinter D, Razafsky DS, Schlager MA, Serra-Marques A, Grigoriev I, Demmers J, Keijzer N, Jiang K, Poser I, Hyman AA, *et al*. (2012). BICD2, dynactin, and LIS1 cooperate in regulating dynein recruitment to cellular structures. Mol Biol Cell 23, 4226–4241.
Tan R, Lam AJ, Tan T, Han J, Nowakowski DW, Vershinin M, Ori-McKenney KM, McKenney RJ (2019). Microtubules gate tau condensation to spatially regulate microtubule functions. Nat Cell Biol 21, 1078–1085.
Tripathy SK, Weil SJ, Chen C, Anand P, Vallee RB, Gross SP (2014). Autoregulatory mechanism for dynactin control of processive and diffusive dynein transport. Nat Cell Biol 16, 1192–1201.
Trokter M, Mucke N, Surrey T (2012). Reconstitution of the human cytoplasmic dynein complex. Proc Natl Acad Sci 109, 20895–20900.
Urnavicius L, Lau CK, Elshenawy MM, Morales-Rios E, Motz C, Yildiz A, Carter AP (2018). Cryo-EM shows how dynactin recruits two dyneins for faster movement. Nature 554, 202–206.
Urnavicius L, Zhang K, Diamant AG, Motz C, Schlager MA, Yu M, Patel NA, Robinson CV, Carter AP (2015). The structure of the dynactin complex and its interaction with dynein. Science 347, 1441–1446.
Zhang K, Foster HE, Rondelet A, Lacey SE, Bahi-Buisson N, Bird AW, Carter AP (2017). Cryo-EM reveals how human cytoplasmic dynein is auto-inhibited and activated. Cell 169, 1303–1314.